Supplementary information

Nucleotide-functionalized graphene nanoribbons for accurate high-speed DNA sequencing

Eugene Paulechka, Tsjerk A. Wassenaar, Kenneth Kroenlein, Andrei Kazakov, and Alex Smolyanitsky

S1. Strain-induced modification of electrical conduction in graphene nanoribbons

The electronic properties of graphene nanoribbons (GNRs) in absence of externally induced strain depend on their width, aspect ratio, purity, edge type (zigzag or armchair) relative to the bias direction [1-6], and the presence of passivation at the edges [7], as well as the passivation content [7, 8]. Particularly relevant to our discussion, the GNR geometry determines the effective operating bias points suitable for strain detection when coherent transport dominates [1]. Further, geometrically perfect edges without chemical passivation are currently unlikely to be obtained experimentally, and thus the appropriate measurement strategy must be determined for a particular GNR.

Nevertheless, the *relative variation* of the electrical current around the baseline values due to deflection-induced strains can be estimated at the order-of-magnitude level for idealized cases. Furthermore, the nanomechanical deflections reported in the main text are for a zigzag-edged GNR and are generally valid for armchair GNRs of similar dimensions. Therefore, our discussion of the strain value estimates is not necessarily limited to the particular GNR type used in our MD simulations. Further, as seen in Eq. (S4) below and mentioned in the main text, a similar nanomechanical response can be obtained from GNRs of varying length and width (provided some requirements on the aspect ratio are met), thus allowing a degree of freedom in varying the dimensions, crucial for the design of the GNR properties in absence of strain. Here

we briefly present the basic mechanisms underlying the effect of uniaxial strains on the electronic properties of GNRs, while the numerical estimates are provided in section S2.

The resistance of a GNR at a given appropriately selected bias point, excluding contact resistance for clarity, in the thermally activated regime is approximated as [9]:

$$R = \frac{R_0}{|t|^2}\left(1 + e^{\frac{E_{gap}}{kT}}\right), \qquad \text{(S1)}$$

where R_0 is the quantum resistance unit, $|t|^2$ is the effective transmission probability for electrons with a given energy E (as dictated by the bias), such that $|E - E_F| > E_{gap}$ (E_F and E_{gap} are the Fermi level and the bandgap, as determined by the GNR dimensions, edge, *etc.*, respectively), and T is the temperature. In the thermally activated conduction regime expected to dominate the water-immersed GNR at room temperature, the effect of strain is primarily due to modification of the number of carriers proportional to $e^{-\frac{E_{gap}}{kT}}$ via strain-induced change of E_{gap}, resulting in $\frac{\delta R}{R} \approx \frac{\delta E_{gap}}{kT}$ (independent of E_{gap} itself in the perturbative approximation), where $\delta E_{gap} \approx 3t_0\varepsilon$, ($t_0 \approx 2.7\ eV$ is the nearest-neighbor electron hopping energy for graphene, ε is the strain), thus yielding $\frac{\delta R}{R} \approx \frac{3t_0\varepsilon}{kT}$. The theoretical tight-binding estimate $\delta E_{gap} \approx 3t_0\varepsilon$ is close to the results obtained with density functional theory calculations for both zigzag and armchair GNRs under uniaxial strain [5].

For completeness, in the T = 0 K limit, Eq. (S1) is effectively replaced by the coherent transport term:

$$R = \frac{R_0}{|t|^2} \qquad \text{(S2)}$$

and the effect of strain is via modification of the effective (quantized) transmission probability $|t|^2$. In this case, the effect of strain on a gateless GNR is negligible [10]. However, around an appropriately selected bias point, strain can indeed be detected in an interferometer-type measurement setup with a relative variation of *R* estimated at $\frac{\delta R}{R} = -\frac{\delta|t|^2}{|t|^2} \approx \frac{h^2}{La_0}$, where *h* is the out-of-plane deflection, *L* is the effective GNR length, and a_0 is the C-C interatomic distance in graphene [10].

In the next sections we estimate the out-of-plane deflection *h* and evaluate the order of magnitude of the changes in resistance induced by the strains due to forces expected in our system.

S2. GNR deflection with lateral pre-strain

As a rough estimate, the maximum out-of-plane deflection *h* of an edge-clamped GNR of length *L* due to force *F* applied at *L/2* is the solution of the following cubic equation:

$$F = \frac{2E_{2D}wh}{L^2}\left(\varepsilon_0 L + \frac{2h^2}{L}\right), \qquad \text{(S3)}$$

where E_{2D}, *w*, and ε_0 are the two-dimensional Young's modulus of graphene, GNR width, and the initial pre-strain along the GNR length, respectively. A reasonable agreement with the simulated data was obtained with $E_{2D} \approx (E_{3D}h_0) = 106\ N/m$, where $E_{3D} = 1.06\ TPa$ and $h_0 = 0.1\ nm$ are the 3-D Young's modulus of graphene and its effective "continuum" thickness, respectively [11].

For *L* = 15.5 nm, *F* = 75 pN, and $\varepsilon_0 = 0.5$ %, Eq. (S3) yields *h* = 2.24 Å, in reasonable agreement with the results in Figs. 3 (a, b) in the main text (results consistent with Fig. 3 (a, b)

were also obtained in MD simulations with the DNA atomic charges set according to AMBER [12]). Without pre-strain ($\varepsilon_0 = 0$), the central deflection is:

$$h = L\left(\frac{F}{4E_{2D}w}\right)^{1/3}, \qquad \text{(S4)}$$

yielding $h_{\varepsilon_0=0}$ = 5.27 Å. The deflection-induced strain in this case is $\varepsilon \approx 2\left(\frac{h}{L}\right)^2 = 0.23$ %, which causes an estimated $\frac{\delta R}{R} \approx \frac{\delta E_{gap}}{kT} = \frac{3t_0\varepsilon}{kT}$ = 71% and $\frac{\delta R}{R} \approx \frac{h^2}{La_0} = 12\%$, according to Eqs. (S1) and (S2), respectively. For the A-T binding with a critical force of *F* = 50 pN, $h_{\varepsilon_0=0}$ = 4.60 Å, yielding the $\frac{\delta R}{R}$ estimates of 32 % and 5.3 %, according to Eqs. (S1) and (S2), respectively.

With the experimentally obtained $E_{2D} = 352\ N/m$ [13], Eq. (S3) underestimates the deflections obtained in our simulations with $\varepsilon_0 = 0.5$ %. However, with lower ε_0, it yields deflections of comparable magnitude, and thus all of the estimates made here remain valid. For example, with $E_{2D} = 352\ N/m$ and $\varepsilon_0 = 0.1$ %, we obtain a deflection value of 1.9 Å for the C-G pair, and thus identical $\frac{\delta R}{R}$ estimates. Without pre-strain, the maximum deflection according to Eq. (S2) is $h_{\varepsilon_0=0} = 3.1$ Å, and thus $\frac{\delta R}{R} \approx \frac{\delta E_{gap}}{kT} = \frac{3t_0\varepsilon}{kT}$ = 24% from Eq. (S1). Within the approximations made, all of these estimates are valid for GNRs of appropriately scaled dimensions.

S3. Additional note on the GNR edge effects

A very narrow GNR, such as the one used in our simulations, would present a region of locally reduced conductance in the nanopore region, given the closeness of the pore edge to the GNR edge. An additional effect on the electrical conductivity thus would arise from the local strain inhomogeneity near the pore, similar to the effects of local inhomogeneous strains shown

elsewhere [1, 14]. Although only demonstrated in vacuum at zero temperature, the electronic properties of a narrow GNR could also be affected by the fact of nucleobase presence in the pore, even without functionalization [15]. However, these effects would be virtually non-existent in a considerably wider GNR at a finite temperature, given that the pore diameter would remain the same. Interestingly, a contribution from the pseudomagnetic field effect could arise in addition to the effects discussed earlier[16] in a wide GNR deflected by an effectively point force at the center.

S4. Effects of rippling

It has been shown previously that the local modulation of the graphene's nearest-neighbor electron hopping energetics by flexural ripples [17] can be described by the emergence of a gauge field [18-20]. An estimate of the time-averaged effect of the ripples can be obtained from considering them as carrier scatterers, which leads to an overall increase of the electrical resistivity [21], in addition to the temporal modulation of the current. In the long-wave approximation, this excess resistivity ρ_r increases with the rippling strength (*e.g.*, in terms of the mean-square out-of-plane displacement $\langle h^2 \rangle$), while its size-scaling properties depend on the rippling Fourier scaling law h_q^2 [21]. Here, we discuss the qualitative effect of FGNR rippling on ρ_r during DNA translocation by considering the wave-vector distributions h_q^2 and the $\langle h^2 \rangle$ averages, as obtained during the passage of G and non-G residues through the FGNR (see section S5 for the calculation details). Shown in Fig. S1 are the h_q^2 distributions for the FGNR at T = 300 K, along with the raw rippling data in the corresponding inset. As shown, the distributions are similar during the passage of G and non-G residues, although *the rippling strength during G passage is consistently lower*. The latter is expected, because even the relatively faint lateral

strain can significantly suppress thermal flexural fluctuations.[22] Direct calculations of $\langle h^2 \rangle$ ($\propto \int h_q^2 \, d\Omega_q$, where $d\Omega_q$ is an area element in the 2-D reciprocal space) confirm this observation, yielding a decrease from 1.63 Å^2 to 1.35 Å^2 during the passage of non-G and G, respectively. An accurate quantitative estimate of $\Delta\rho_r/\rho_r$ due to FGNR deflection induced strain would crucially depend on the dimensions, as well as the fabrication methods of an experimentally relevant GNR. However, the relatively high sensitivity of the ripple scattering mechanism to $\langle h^2 \rangle$ (and thus to deflection-induced strain) can be revealed via previously estimated $\rho_r \propto n_r/n_c$ [21], where $n_r \propto \langle h^2 \rangle^2$ and $n_c \propto e^{-\frac{E_{gap}}{kT}}$ is the effective sheet density of the scatterers and charge carriers, respectively. As a result of excess strain due to G-induced FGNR deflection, $\frac{\Delta\rho_r}{\rho_r} \propto \frac{\Delta n_r}{n_r} - \frac{\Delta n_c}{n_c}$. Here, $n_r \propto \langle h^2 \rangle^2$ is considerably reduced (by ~30 %, from the $\langle h^2 \rangle$ estimates above) and $\Delta n_c/n_c \propto -\frac{3t_0\varepsilon}{kT} < 0$ due to strain-induced bandgap modulation, estimated at ~10 % above. The net result of this competition between strain-induced decreased scattering and a decrease in the number of charge carriers is reduction of ρ_r by ~20 %. Therefore, if ripple scattering is expected to significantly contribute to the overall resistance in a given GNR, the described effect of strain-induced ripple suppression may become an additional mechanism contributing to the net current variation.

S5. Out-of-plane rippling statistics

For the *t*-th MD frame, an individual h_q^2 distribution was calculated directly from the atomic population of the FGNR as the corresponding 2-D Fourier transform of $(z_i - \bar{z}_t)^2$, where z_i is the *i*-th atom's position along Z and $\bar{z}_t$ is the local plane level at time *t*. The distributions h_q^2

were presented as *averages of distributions* over multiple frames for each translocation portion (G and non-G), similarly to the statistical data presented elsewhere [17, 23, 24].

The *t*-th per-frame average from *N* atoms in the GNR is

$$\langle h_t^2 \rangle = \frac{1}{N-1} \sum_N (z_i - \bar{z}_t)^2, \qquad \text{(S5)}$$

and the grand average per multiple frames is calculated as $\langle h^2 \rangle = \frac{1}{\tau} \sum_\tau \langle h_t^2 \rangle$. Note that for a membrane deflected at the center, the use of a global "plane level" $\bar{z}_t = \frac{1}{N} \sum_N z_i$ is incorrect. Therefore, we used the local plane level $\bar{z}_{t,i}$ equal to the *per-atom* running time-average obtained from an infinite impulse response (IIR) filter. Ripple suppression was independently confirmed by using Eq. (S5), while calculating $\bar{z}_{t,i}$ from a second-order polynomial surface fit at every MD frame. The data in Fig. S1 and the grand averages discussed in section S4 were calculated over τ = 20 ns long periods of G and non-G translocation (see inset of Fig. S1; translocation data from Fig. 3 (b)). The frame spacing was 50 ps, resulting in a total of 400 frames used in the averaging for each passage.

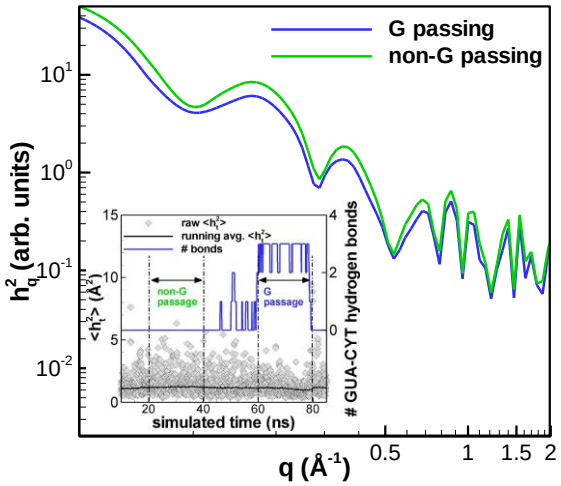

Figure S1. FGNR rippling distributions h_q^2 during the passage of G and non-G nucleobases. The inset shows the averaging regions, the raw $\langle h_t^2 \rangle$ data (as defined in section S4), as well as the $\langle h_t^2 \rangle$ running average data.

References

1. Cosma, D.A., et al., *Strain-induced modifications of transport in gated graphene nanoribbons.* Physical Review B, 2014. **90**(24): p. 245409.
2. Nakada, K., et al., *Edge state in graphene ribbons: Nanometer size effect and edge shape dependence.* Physical Review B, 1996. **54**(24): p. 17954-17961.
3. Barone, V., O. Hod, and G.E. Scuseria, *Electronic Structure and Stability of Semiconducting Graphene Nanoribbons.* Nano Letters, 2006. **6**(12): p. 2748-2754.
4. Yoon, Y. and J. Guo, *Effect of edge roughness in graphene nanoribbon transistors.* Applied Physics Letters, 2007. **91**(7): p. 073103.
5. Li, Y., et al., *Strain effects in graphene and graphene nanoribbons: The underlying mechanism.* Nano Research, 2010. **3**(8): p. 545-556.
6. Son, Y.-W., M.L. Cohen, and S.G. Louie, *Energy Gaps in Graphene Nanoribbons.* Physical Review Letters, 2006. **97**(21): p. 216803.
7. Lu, Y.H., et al., *Effects of edge passivation by hydrogen on electronic structure of armchair graphene nanoribbon and band gap engineering.* Applied Physics Letters, 2009. **94**(12): p. 122111.
8. Zeng Yong-Chang, T.W., Zhang Zhen-Hua, *Electronic properties of graphene nanoribbons with periodical nanoholes passivated by oxygen.* Acta Physica Sinica, 2013. **62**(23): p. 236102-236102.
9. Minot, E.D., et al., *Tuning Carbon Nanotube Band Gaps with Strain.* Physical Review Letters, 2003. **90**(15): p. 156401.
10. Isacsson, A., *Nanomechanical displacement detection using coherent transport in graphene nanoribbon resonators.* Physical Review B, 2011. **84**(12): p. 125452.

11. Scarpa, F., S. Adhikari, and A.S. Phani, *Effective elastic mechanical properties of single layer graphene sheets.* Nanotechnology, 2009. **20**(6): p. 065709.
12. Duan, Y., et al., *A point-charge force field for molecular mechanics simulations of proteins based on condensed-phase quantum mechanical calculations.* Journal of Computational Chemistry, 2003. **24**(16): p. 1999-2012.
13. Booth, T.J., et al., *Macroscopic Graphene Membranes and Their Extraordinary Stiffness.* Nano Letters, 2008. **8**(8): p. 2442-2446.
14. Smolyanitsky, A. and V.K. Tewary, *Simulation of lattice strain due to a CNT–metal interface.* Nanotechnology, 2011. **22**(8): p. 085703.
15. Nelson, T., B. Zhang, and O.V. Prezhdo, *Detection of Nucleic Acids with Graphene Nanopores: Ab Initio Characterization of a Novel Sequencing Device.* Nano Letters, 2010. **10**(9): p. 3237–3242.
16. Fogler, M.M., F. Guinea, and M.I. Katsnelson, *Pseudomagnetic Fields and Ballistic Transport in a Suspended Graphene Sheet.* Physical Review Letters, 2008. **101**(22).
17. Fasolino, A., J.H. Los, and M.I. Katsnelson, *Intrinsic ripples in graphene.* Nature Materials, 2007. **6**(11): p. 858 - 861.
18. Morozov, S.V., et al., *Strong Suppression of Weak Localization in Graphene.* Physical Review Letters, 2006. **97**(1): p. 016801.
19. Eun-Ah, K. and A.H.C. Neto, *Graphene as an electronic membrane.* EPL (Europhysics Letters), 2008. **84**(5): p. 57007.
20. Abedpour, N., et al., *Roughness of undoped graphene and its short-range induced gauge field.* Physical Review B, 2007. **76**(19): p. 195407.
21. Katsnelson, M.I. and A.K. Geim, *Electron scattering on microscopic corrugations in graphene.* Philosophical Magazine, 2008. **366**(1863): p. 195-204.
22. Gao, W. and R. Huang, *Thermomechanics of monolayer graphene: Rippling, thermal expansion and elasticity.* Journal of the Mechanics and Physics of Solids, 2014. **66**: p. 42-58.
23. Los, J.H., et al., *Scaling properties of flexible membranes from atomistic simulations: Application to graphene.* Physical Review B, 2009. **80**(12): p. 121405.
24. Smolyanitsky, A., *Effects of thermal rippling on the frictional properties of free-standing graphene.* RSC Advances, 2015. **5**(37): p. 29179-29184.